

Nanoscale microwave imaging with a single electron spin in diamond

This content has been downloaded from IOPscience. Please scroll down to see the full text.

2015 New J. Phys. 17 112001

(<http://iopscience.iop.org/1367-2630/17/11/112001>)

View [the table of contents for this issue](#), or go to the [journal homepage](#) for more

Download details:

IP Address: 131.152.211.50

This content was downloaded on 23/02/2017 at 14:07

Please note that [terms and conditions apply](#).

You may also be interested in:

[Magnetometry with nitrogen-vacancy defects in diamond](#)

L Rondin, J-P Tetienne, T Hingant et al.

[Magnetic field imaging with nitrogen-vacancy ensembles](#)

L M Pham, D Le Sage, P L Stanwix et al.

[Topical review: spins and mechanics in diamond](#)

Donghun Lee, Kenneth W Lee, Jeffrey V Cady et al.

[Influence of Microwave Detuning on Ramsey Fringes of a Single Nitrogen Vacancy Center Spin in Diamond](#)

Hu Xin, Liu Gang-Qin, Xu Zhang-Cheng et al.

[Vector magnetic field sensing by a single nitrogen vacancy center in diamond](#)

X.-D. Chen, F.-W. Sun, C.-L. Zou et al.

[All-optical magnetic resonance of high spectral resolution using a nitrogen-vacancy spin in diamond](#)

Zhen-Yu Wang, Jian-Ming Cai, Alex Retzker et al.

[Hyperfine-enhanced gyromagnetic ratio of a nuclear spin in diamond](#)

S Sangtawesin, C A McLellan, B A Myers et al.

[Magnetic-field-dependent photodynamics of single NV defects in diamond: an application to qualitative all-optical magnetic imaging](#)

J-P Tetienne, L Rondin, P Spinicelli et al.



FAST TRACK COMMUNICATION

Nanoscale microwave imaging with a single electron spin in diamond

OPEN ACCESS

RECEIVED

10 August 2015

REVISED

25 September 2015

ACCEPTED FOR PUBLICATION

13 October 2015

PUBLISHED

3 November 2015

Content from this work
may be used under the
terms of the [Creative
Commons Attribution 3.0
licence](#).

Any further distribution of
this work must maintain
attribution to the
author(s) and the title of
the work, journal citation
and DOI.

Patrick Appel^{1,3}, Marc Ganzhorn^{1,3}, Elke Neu² and Patrick Maletinsky¹¹ Department of Physics, University of Basel, Klingelbergstrasse 82, Basel CH-4056, Switzerland² Saarland University, Experimentalphysik, Campus E2.6, D-66123 Saarbruecken, Germany³ These authors contributed equally to this work.**Keywords:** microwave imaging, nanoscale magnetic field sensing, nitrogen vacancy center, diamondSupplementary material for this article is available [online](#)**Abstract**

We report on imaging of microwave (MW) magnetic fields using a magnetometer based on the electron spin of a nitrogen vacancy (NV) center in diamond. We quantitatively image the magnetic field generated by high frequency (GHz) MW current with nanoscale resolution using a scanning probe technique. Together with a shot noise limited MW magnetic field sensitivity of $680 \text{ nT Hz}^{-1/2}$ our room temperature experiments establish the NV center as a versatile and high performance tool for MW imaging, which furthermore offers polarization selectivity and broadband capabilities. As a first application of this scanning MW detector, we image the MW stray field around a stripline structure and thereby locally determine the MW current density with a MW current sensitivity of a few $\text{nA Hz}^{-1/2}$.

1. Introduction

Imaging and detecting microwave (MW) fields constitutes a highly relevant element for engineering of future MW devices as well as for applications in atomic and solid state physics. For instance cavity quantum electrodynamics experiments with atoms [1, 2] and superconducting qubits [3, 4] or the coherent control of quantum magnets [5] and quantum dots [6] are based on manipulating quantum systems with MW electric or magnetic fields. Precise control and knowledge of the spatial distribution of the MW near field is thereby essential to achieve optimal device performance. Also, magnetic systems are known to exhibit a large variety of collective magnetic excitations, including spin waves [7] or excitations in frustrated magnets [8, 9]. Imaging such magnetic excitations on the nanoscale is a crucial step towards their fundamental understanding and the development of new spintronics devices, such as magnonic waveguides [10] or domain wall racetrack memories [11]. As a consequence, various techniques have been designed to image MW electric and magnetic fields, including scanning near field microscopy [12–14], micro-Brillouin light scattering [15], superconducting quantum interference devices [16] or imaging with atomic vapor cells [17–19] or ultracold atoms [20]. With only a few exceptions [15], most of these techniques however lack a nanoscale spatial resolution or are restricted to operation in cryogenic or vacuum environments.

MW magnetic field imaging using the electronic spin of a single nitrogen vacancy (NV) center in diamond offers a promising alternative. The NV center is an optically active lattice point defect in diamond with a $S = 1$ ground state manifold. Its atomic size, exceptionally long coherence times, optical initialization and readout of the spin state make the NV center an ideal sensor for DC magnetic fields under ambient conditions [21–25]. Recently, magnetometry of MW magnetic fields has been demonstrated using a NV spin in bulk diamond [26], with a resulting MW magnetic field sensitivity of one $\mu\text{T Hz}^{-1/2}$. However, the bulk NV centers employed in [26] severely restricted spatial resolution in imaging, and in particular do not allow for nanoscale imaging of MW near fields, which remains an outstanding challenge for NV-based MW imaging. In this letter, we address this issue and demonstrate the first nanoscale MW imaging using a scanning NV magnetometer [27]. Our proof-of-

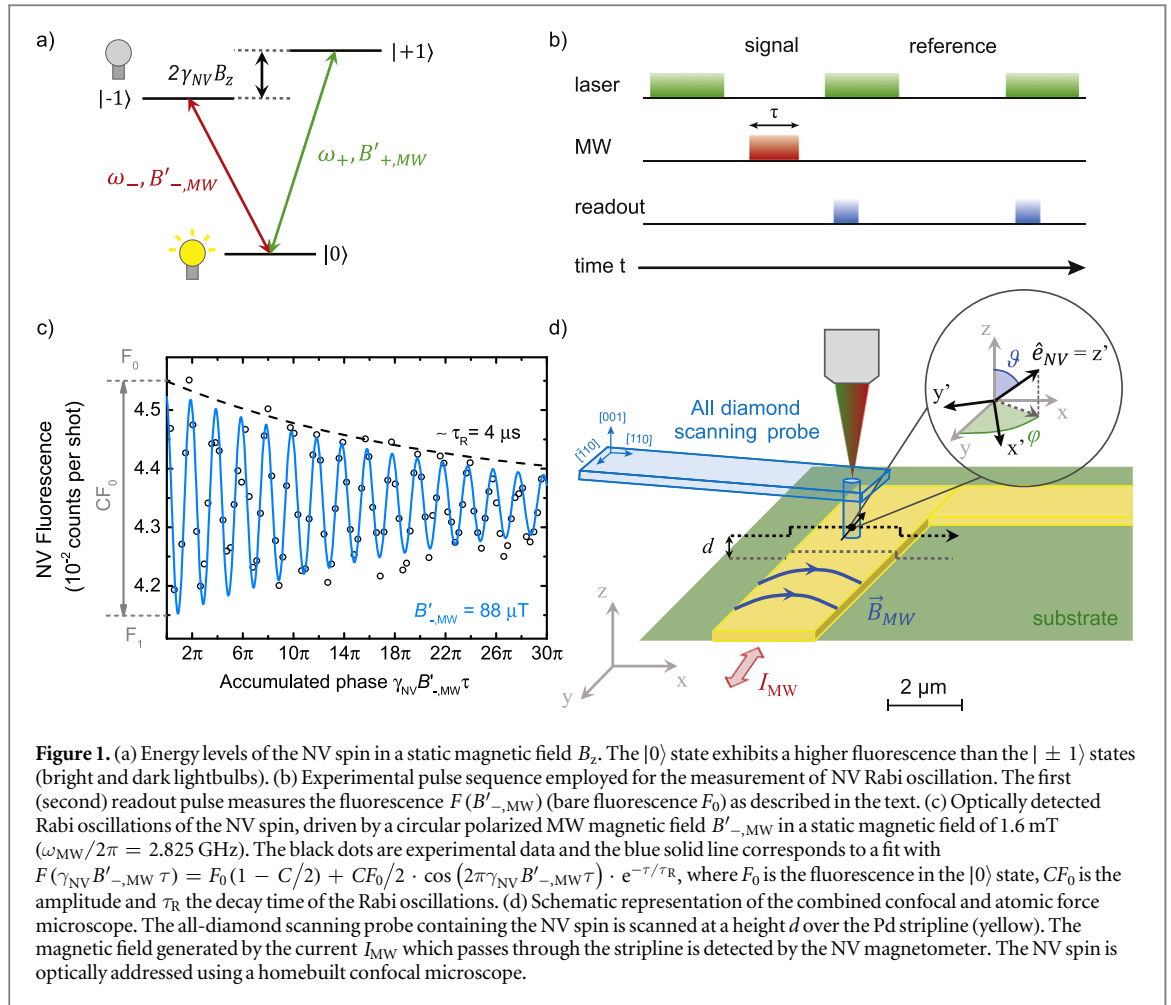


Figure 1. (a) Energy levels of the NV spin in a static magnetic field B_z . The $|0\rangle$ state exhibits a higher fluorescence than the $|\pm 1\rangle$ states (bright and dark lightbulbs). (b) Experimental pulse sequence employed for the measurement of NV Rabi oscillation. The first (second) readout pulse measures the fluorescence $F(B'_{-,MW})$ (bare fluorescence F_0) as described in the text. (c) Optically detected Rabi oscillations of the NV spin, driven by a circularly polarized MW magnetic field $B'_{-,MW}$ in a static magnetic field of 1.6 mT ($\omega_{MW}/2\pi = 2.825$ GHz). The black dots are experimental data and the blue solid line corresponds to a fit with $F(\gamma_{NV}B'_{-,MW}\tau) = F_0(1 - C/2) + CF_0/2 \cdot \cos(2\pi\gamma_{NV}B'_{-,MW}\tau) \cdot e^{-\tau/\tau_R}$, where F_0 is the fluorescence in the $|0\rangle$ state, CF_0 is the amplitude and τ_R the decay time of the Rabi oscillations. (d) Schematic representation of the combined confocal and atomic force microscope. The all-diamond scanning probe containing the NV spin is scanned at a height d over the Pd stripline (yellow). The magnetic field generated by the current I_{MW} which passes through the stripline is detected by the NV magnetometer. The NV spin is optically addressed using a homebuilt confocal microscope.

concept imaging experiments were performed on a prototypical MW circuit—a micron-scale MW stripline—and yield nanoscale resolution combined with shot noise limited MW magnetic field sensitivities in the range of a few hundred nT Hz^{-1/2}.

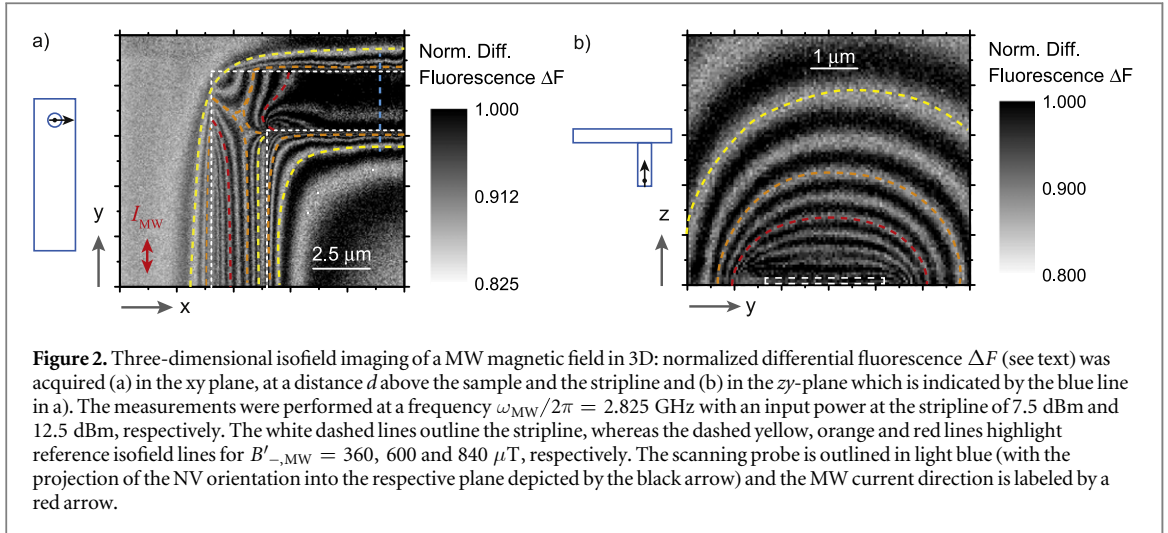
2. MW magnetic field imaging with NV centers in diamond

2.1. Detection principle

Our MW magnetic field detection is based on the ability of the MW field to drive coherent Rabi oscillations between the $|0\rangle$ and $|\pm 1\rangle$ spin-states of the NV center (figures 1(a)–(c)). Selection rules impose that within the rotating wave approximation (RWA), the transition $|0\rangle \rightarrow |\pm 1\rangle$ is only excited by a circularly polarized MW field σ_{\pm} . Due to the large NV spin splitting and the comparably weak microwave field amplitudes, the RWA holds to an extremely good extent in the experiments described here. An arbitrarily polarized MW field resonant with either the $|0\rangle \rightarrow |+1\rangle$ or $|0\rangle \rightarrow |-1\rangle$ transition therefore leads to an oscillation of the population between the two involved spin states, at a frequency $\Omega_{\pm}/2\pi = \gamma_{NV}B'_{\pm, MW}$, where $B'_{\pm, MW}$ is the (right-) left-handed circularly polarized component of the MW field in a plane perpendicular to the NV axis and $\gamma_{NV} = 28$ kHz μT^{-1} the NV gyromagnetic ratio. Measuring Ω_{\pm} by an appropriate experimental sequence (figure 1(b)) thus allows one to directly determine the amplitude of the driving MW magnetic field in a circularly polarized basis (figure 1(c)).

The NV spin we employ for MW imaging is located at the apex of an all diamond scanning probe (figure 1(d)), obtained in a series of fabrication steps, including low energy ion implantation, electron beam lithography and inductively coupled reactive ion etching [27]. In order to perform MW magnetic field imaging, the diamond scanning probe is integrated in a homebuilt combined confocal (CFM) and atomic force microscope (AFM) [27]. The AFM allows scanning of the NV spin in close proximity to a sample while the CFM is employed to optically read out the NV center spin state (figure 1(d)).

We demonstrate the performance of our MW magnetic field imaging on the MW stripline structure illustrated in figure 1(d). The 2.5 μm wide MW stripline is patterned onto an undoped Si substrate covered with



300 nm of SiO_2 by electron beam lithography and evaporation of 60 nm of Pd. A MW source (Rhode & Schwarz SMB 100A) is used to drive a MW current I_{MW} with a frequency in the GHz range through the stripline. The right-angled stripline we employ thereby generates a highly inhomogeneous MW magnetic field with a nontrivial field distribution which is largely linearly polarized⁴. This arrangement is therefore ideal to demonstrate spatial resolution and MW magnetic field sensitivity of our imager.

In the following, we demonstrate imaging of the σ_- -component of the MW magnetic field ($\omega_{MW}/2\pi = 2.825$ GHz) generated by the stripline. To that end, we tune the sensing frequency $\omega_-/2\pi = 2.87$ GHz $-\gamma_{NV}B_z$ of the $|0\rangle \rightarrow |-1\rangle$ transition via a static magnetic field B_z to the frequency $\omega_{MW}/2\pi$ of the MW field (see figure 1(a)). In analogy, the σ_+ -component of the MW magnetic field can in principle be addressed by changing the external magnetic field B_z such that the $|0\rangle \rightarrow |+1\rangle$ transition of the NV center is resonant with the frequency of the MW field to be imaged. However, we did not perform such an experiment, as for the device under test the MW magnetic field contains equal contributions of circular polarizations and would therefore not provide any polarization contrast in imaging (see footnote 4).

2.2. Isofield imaging mode

In the first imaging mode, we perform imaging of equi-magnetic field lines of constant amplitude $B'_{-,MW}$. For a fixed MW pulse length τ_0 , the accumulated phase (pulse area) in the Rabi oscillation and thus the population difference between $|0\rangle$ and $|-1\rangle$ depends on the local MW magnetic field $B'_{-,MW}$ (figure 1(b)–(c)). While scanning the NV spin at a distance d over the stripline, one can therefore monitor variations of the MW magnetic field via changes in the NV fluorescence F (figure 2).

In order to correct for fluorescence changes arising from potential near field effects [27–29] while scanning, we simultaneously record the bare fluorescence rate F_0 of the $|0\rangle$ state to yield the normalized differential fluorescence, $\Delta F = [F(B'_{-,MW}) - F_0]/F_0$.

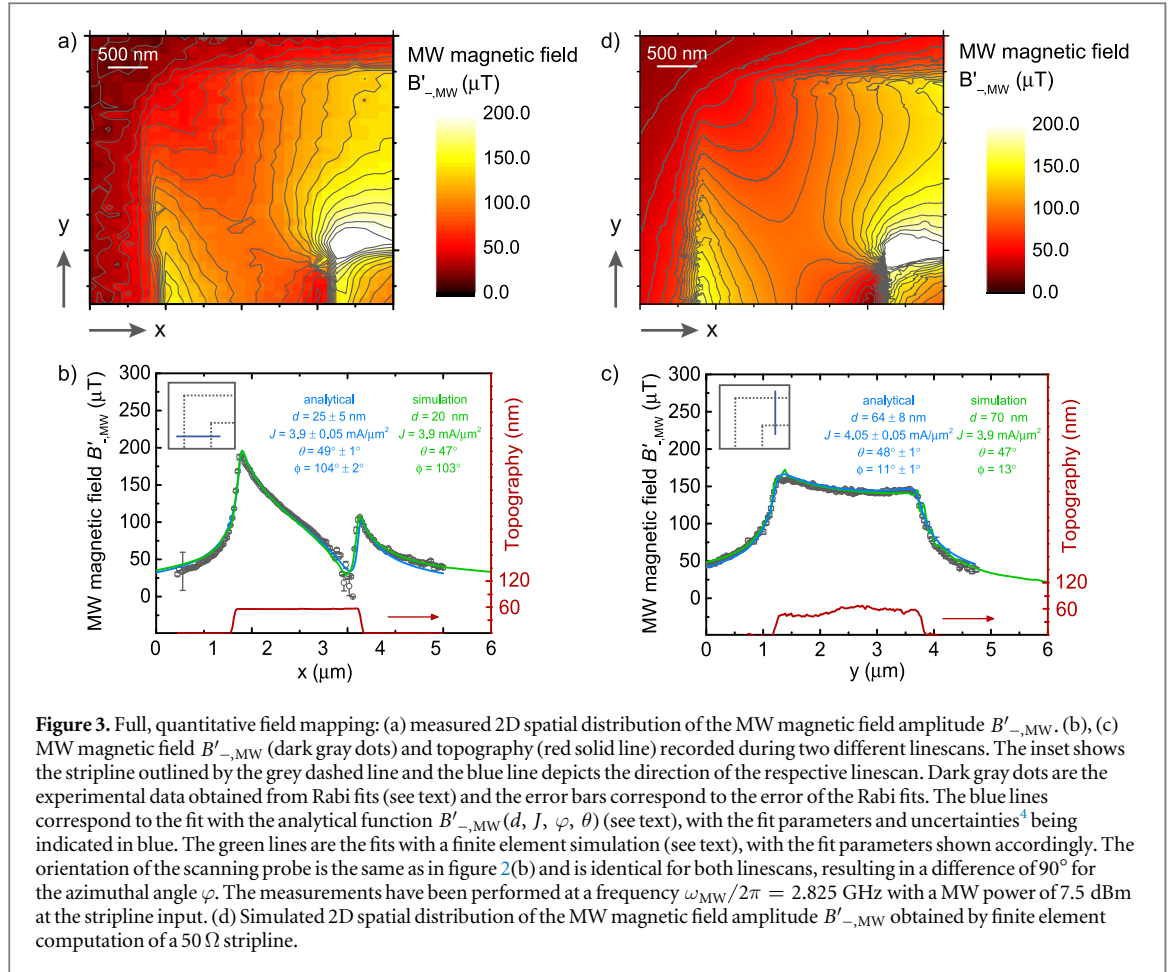
Figure 2(a) shows ΔF recorded in the xy -plane in AFM contact (corresponding to a height d of the NV spin above the stripline) with $\tau_0 = 300$ ns. Each bright fringe corresponds to an integer multiple of 2π of accumulated phase of the NV Rabi oscillations. Consequently, the bright fringes represent isofield lines of $B'_{-,MW}$, which are spaced by $2\pi/\gamma_{NV}\tau_0 = 120 \mu\text{T}$. To avoid ambiguities in assigning the correct value of $B'_{-,MW}$ to each measured field line, we separately measured $B'_{-,MW}$ for several reference lines. The references for $B'_{-,MW} = 360, 600$ and $840 \mu\text{T}$ are highlighted in yellow, orange and red, respectively in figure 2(a).

The versatility and stability of our microscope allows us to further image MW magnetic fields in all three-dimensions and in particular as a function of distance to the sample. To that end, we release AFM force feedback and record the MW magnetic field image by scanning the sample in a plane orthogonal to the MW current (figure 2(b)). In analogy to figure 2(a), we attribute a MW magnetic field amplitude to each isofield line as shown in figure 2(b).

2.3. Full field imaging mode

While providing a fast and straightforward method for nanoscale imaging of MW magnetic fields, our method for iso-field imaging suffers from limitations in regions of high magnetic field gradients. This is particularly appreciable near the edges of our stripline (figure 2(a)), where individual field lines are hard to distinguish and

⁴ See supplementary material for further details.



identification of the measured isofield lines becomes intractable. In order to overcome this limitation, we extended our imaging capabilities to directly determine $B'_{-,MW}$ at each point throughout the scan (figure 3). For this, we measured NV Rabi oscillations at each pixel in the scan range and determined $B'_{-,MW}$ by a sinusoidal fit to each of these traces. Figure 3(a) depicts the resulting image of $B'_{-,MW}$ measured above the corner of the stripline imaged in figure 2(a). From this data, we also extract iso-field lines as highlighted by gray solid lines in figure 3(a). For the quantitative analysis of our results, which we provide below, we further used this imaging method to record linecuts of $B'_{-,MW}$ as depicted in figures 3(b) and (c).

The measured distributions of $B'_{-,MW}$ depends on the orientation (φ, θ) and the position $\vec{r} = (x, y, z)$ of the NV spin with respect to the MW current⁴ (see also figure 1). Assuming an infinitely thin stripline ($t \ll w$) in vacuum with a homogeneous MW current density J oriented parallel to the stripline, the MW magnetic field profiles in figures 3(b) and (c) can be described by an analytical function $B'_{-,MW}(d, J, \varphi, \theta)$, with d, J, φ, θ as free parameters. We note that our assumption of a homogenous current⁴ distribution is justified by the fact that the skin-depth of Pd at 2.825 GHz is larger than the stripline-width and is further corroborated by our numerical simulations⁴. The resulting fits (blue lines in figures 3(b) and (c)) are in excellent agreement with the experimental data (dark gray dots in figures 3(b) and (c)). In addition, we have numerically computed in a finite element simulation the MW magnetic field amplitude, assuming a MW current in a stripline (width $w = 2.5 \mu\text{m}$, thickness $t = 60$ nm) on 300 nm of SiO_2 ⁴. The best fit to the experimental data (green lines in figure 3(b) and (c)) is achieved with parameters d, J, φ, θ (green insets) that are almost identical to the analytical fit parameters (blue insets). Finally, we also numerically determined the full two-dimensional distribution of the MW magnetic field in a finite element simulation (figure 3(d)), using the distance and orientation of the NV spin determined in figure 3(b)⁴. For most of the scanned area, the experimental data (figure 3(a)) are in excellent agreement with the simulation (figure 3(d)), which further establishes the reliability of our method.

3. Spatial resolution and MW field sensitivity

The accurate determination of the NV-to-sample distance $d = 25 \pm 5$ nm that our method provides is relevant for various aspects of our work and NV-based sensing in general. First and foremost, d determines the spatial resolution in imaging the sources of magnetic fields [27, 30], which we thus estimate to be ~ 25 nm. Moreover,

the distance links the MW current in the stripline to the MW magnetic field seen by the NV spin and therefore sets the sensitivity with which one can detect a MW current in the sample. With $d \sim 25$ nm and the magnetic field sensitivity determined below, we find a MW current sensitivity of our NV magnetometer of ~ 300 nA Hz $^{-1/2}$ for an infinitely thin, current-carrying wire. Note that for the data set presented in figure 3(c), we find $d = 64 \pm 5$ nm, significantly larger than the value of $d = 25 \pm 5$ nm, which we determine for all the other data presented in this work. We attribute this discrepancy to contaminations on the diamond tip that has accumulated throughout the course of our experiments⁴—removing these contaminants or working with a fresh tip should restore d to its original value.

We now estimate the photon shot noise limited sensitivity of the NV spin determined by $\eta_{\text{photon}} = \sqrt{2e} / (\pi \gamma_{\text{NV}} C \sqrt{F_0 \tau_R})$, with F_0 , C and τ_R as defined earlier (see figure 1 and ⁴). For the NV spin used in our experiments, we find $\eta_{\text{photon}} = 680$ nT Hz $^{-1/2}$ at 2.825 GHz⁴. It should be noted that in general the decay time of the Rabi oscillation τ_R is itself a function of the Rabi frequency (and thus of B'_{MW}) [31]. While a general expression for η_{photon} is therefore difficult to obtain, it is instructive to consider the two limits of low and high Rabi frequencies with respect to $1/T_2^*$, where the decay time is given by $\tau_R = T_2^*$ and T_1 , respectively. For typical values of NV centers in ultrapure diamond ($T_2^* \sim 1$ μ s and $T_1 \sim 1$ ms) one then finds $\eta_{\text{photon}} \sim 1.4$ μ T Hz $^{-1/2}$ and $\eta_{\text{photon}} \sim 40$ nT Hz $^{-1/2}$ respectively. Additionally, we note that while coherent detection of MW fields through Rabi oscillations is limited by τ_R , incoherent detection of these fields is limited by T_1 only. Performing such incoherent MW imaging (also referred to as relaxation-imaging [32, 33]) would thus allow us to reach the highest sensitivities also in the limit of low Rabi frequencies. The sensitivity could be further enhanced by improving the Rabi decay time τ_R using isotopically enriched diamond [21, 34] and by optimizing the photon collection efficiency using alternative tip geometries [35] or scanning probes made from [111] oriented diamond material [36]. In addition, the MW magnetic field sensitivity can be estimated from the full, quantitative field measurement (figure 3) and is given by $\eta_{\text{meas}} = \delta B'_{-, \text{MW}} \sqrt{T}$, where $\delta B'_{-, \text{MW}}$ is the smallest measurable MW magnetic field, i.e. the fitting error to the Rabi fits, and T the measurement time for each data point. For the values extracted from figure 3 we obtain a sensitivity of $\eta_{\text{meas}} = 15$ μ T Hz $^{-1/2}$,⁴ which is larger than the shot-noise limited sensitivity quoted above. This discrepancy is explained by the fact that for the measurement shown in figure 3, we recorded full Rabi oscillations for each point of the scan, i.e. most of the data was taken for evolution times τ , which do not yield optimal measurement sensitivities⁴.

4. Conclusion and outlook

In conclusion, we have established scanning NV center spins as a valuable resource to sensitively detect and image MW magnetic fields on the nanoscale. Our results indicate an imaging resolution of ~ 25 nm together with a shot noise limited MW magnetic field sensitivity of 680 nT Hz $^{-1/2}$, resulting in a sensitivity to the generating currents of few nA Hz $^{-1/2}$ all at frequencies ~ 3 GHz. Extending the bandwidth of detection to the range above 20 GHz can be achieved by placing our microscope in a sufficiently strong magnetic field [37] and would have profound impact for applications in MW device characterization, as currently available field imaging techniques cannot operate in this frequency range [38]. It should be noted that detection of microwave fields through Rabi oscillations has also been implemented for ⁸⁷Rb vapor cells [17–20]. Such devices operate with tens of μ m spatial resolution over a mm to cm detection window [39], compared to our nanoscale spatial resolution over a tens of μ m detection window, and thus provide a complementary wide field imaging tool to our NV scanning magnetometers. Finally, recent experiments have demonstrated that spin wave excitations in nanomagnetic systems can be addressed via MW NV magnetometry [40]. There external DC magnetic fields are used to bring the spin wave excitation frequency into resonance with the NV spin transition and thus enables a detection of the spin wave amplitude via the NV Rabi frequency. Combining this detection scheme with our ability to image MW magnetic fields at nanoscale resolution would therefore form an exciting avenue that could allow for real space imaging of spin wave excitation in nanomagnets [41] or skyrmion core dynamics [42].

Acknowledgments

We gratefully acknowledge financial support through the NCCR QSIT, a competence center funded by the Swiss NSF, and through SNF Grant No. 200021 143697/1 and Grant No. 155845. This research has been partially funded by the European Commission's 7. Framework Program (FP7/2007-2013) under grant agreement No. 611143 (DIADEMS). EN acknowledges funding via the NanoMatFutur program of the German ministry of education and research. We thank B Shields, A Barfuss, A Horsley and P Treutlein for fruitful discussions.

References

- [1] Kaluzny Y, Goy P, Raimond J and Haroche S 1983 *Phys. Rev. Lett.* **51** 1175
- [2] Raimond J, Brune M and Haroche S 2001 *Rev. Mod. Phys.* **73** 565
- [3] Walraff A, Schuster D, Blais A, Frunzie L, Huang R S, Majer J, Kumar S, Girvin S and Schoelkopf R 2004 *Nature* **431** 162
- [4] You J and Nori F 2011 *Nature* **474** 589
- [5] Thiele S, Balestro F, Ballou R, Klyatskaya S, Ruben M and Wernsdorfer W 2014 *Science* **344** 1135
- [6] Koppens F, Buizert C, Tielrooij K, Vink I, Nowack K, Meunier T, Kouwenhoven L and Vandersypen L 2006 *Nature* **442** 766
- [7] Sparks M 1964 *Ferromagnetic-Relaxation Theory* (New York: McGraw-Hill)
- [8] Schollwoeck U, Richter J, Farnell D J J and Bishop R F 2004 *Quantum Magnetism* (Berlin: Springer)
- [9] Balents L 2010 *Nature* **464** 199
- [10] Garcia-Sanchez F, Borys P, Soucaille R, Adam J P, Stamps R L and Kim J V 2015 *Phys. Rev. Lett.* **114** 247206
- [11] Parkin S, Hayashi M and Thomas L 2008 *Science* **320** 190–4
- [12] Agrawal V, Neuzil P and van der Weide D W 1997 *Appl. Phys. Lett.* **71** 2343–5
- [13] Lee S C, Vlahacos C P, Feenstra B J, Schwartz A, Steinhauer D E, Wellstood F C and Anlage S M 2000 *Appl. Phys. Lett.* **77** 4404–6
- [14] Rosner B and van der Weide D W 2003 *Rev. Sci. Instrum.* **73** 2505
- [15] Sebastian T, Schultheiss K, Obry B, Hillebrands B and Schultheiss H 2015 *Frontiers Phys.* **3** 35
- [16] Black R C, Wellstood F C, Dantsker E, Miklich A H, Koelle D, Ludwig F and Clarke J 1995 *Appl. Phys. Lett.* **66** 1267
- [17] Boehi P and Treutlein P 2012 *Appl. Phys. Lett.* **101** 181107
- [18] Horsley A, Du G, Pellaton M, Affolderbach C, Mileti G and Treutlein P 2013 *Phys. Rev. A* **88** 063407
- [19] Affolderbach C, Du G X, Bandi T, Horsley A, Treutlein P and Mileti G 2015 *IEEE Trans. Instrum. Meas.* **PP** 1
- [20] Boehi P, Riedel M, Haensch T and Treutlein P 2010 *Appl. Phys. Lett.* **97** 051101
- [21] Rondin L, Tetienne J P, Hingant T, Roch J F, Maletinsky P and Jacques V 2014 *Rep. Prog. Phys.* **77** 056503
- [22] Degen C L 2008 *Appl. Phys. Lett.* **92** 243111
- [23] Taylor J, Cappellaro P, Childress L, Jiang L, Budker D, Hemmer P, Walsworth R, Yacoby A and Lukin M 2008 *Nat. Phys.* **4** 810
- [24] Maze J *et al* 2008 *Nature* **455** 644
- [25] Balasubramanian G *et al* 2008 *Nature* **455** 648
- [26] Wang P, Yuan Z, Huang P, Rong X, Wang M, Xu X, Duan C, Ju C, Shi F and Du J 2015 *Nat. Commun.* **6** 6631
- [27] Maletinsky P, Hong S, Grinolds M S, Haussmann B, Lukin M D, Walsworth R L, Loncar M and Yacoby A 2012 *Nat. Nanotechnology* **7** 320
- [28] Tetienne J P, Rondin L, Spinicelli P, Chipaux M, Debuisschert T, Roch J and Jacques V 2012 *New J. Phys.* **14** 103033
- [29] Anger P, Bharadwaj P and Novotny L 2006 *Phys. Rev. Lett.* **96** 113002
- [30] Hingant T, Tetienne J, Martinez L, Garcia K, Ravelosona D, Roch J F and Jacques V 2015 *Phys. Rev. Appl.* **4** 014003
- [31] Slichter C 1996 *Principles of Magnetic Resonance* (Berlin: Springer)
- [32] Pelliccione M, Myers B A, Pascal L M A, Das A and Bleszynski Jayich A C 2014 *Phys. Rev. Appl.* **2** 054014
- [33] Tetienne J-P, Hingant T, Rondin L, Cavailles A, Mayer L, Dantelle G, Gacoin T, Wrachtrup J, Roch J and Jacques V 2013 *Phys. Rev. B* **87** 235436
- [34] Balasubramanian G *et al* 2009 *Nat. Mater.* **8** 383–7
- [35] Momenzadeh S, Stoehr R, de Oliveira F, Brunner A, Denisenko A, Yang S, Reinhard F and Wrachtrup J 2015 *Nano Lett.* **15** 165–9
- [36] Neu E, Appel P, Ganzhorn M, Miguel-Snchez J, Lesik M, Mille V, Jacques V, Tallaire A, Achard J and Maletinsky P 2014 *Appl. Phys. Lett.* **104** 153108
- [37] Stepanov V, Cho F H, Abeywardana C and Takahashi S 2015 *Appl. Phys. Lett.* **106** 063111
- [38] Sayil S, Kerns D and Kerns S 2005 *IEEE Trans. Instrum. Meas.* **54** 2082
- [39] Horsley A, Du G and Treutlein P 2015 Widefield microwave imaging in alkali vapor cells with sub-100 μm resolution, (accepted)
- [40] van der Sar T, Casola F, Walsworth R and Yacoby A 2015 *Nat. Commun.* **6** 7886
- [41] Spinelli A, Bryant B, Delgado F, Fernandez-Rossier J and Otte A 2014 *Nat. Mater.* **13** 782–5
- [42] Nagaosa N and Tokura Y 2013 *Nat. Nanotechnology* **8** 899